

© 2020. P. Stroeven, M. Slowik.

This is an open-access article distributed under the terms of the Creative Commons Attribution-NonCommercial-NoDerivatives License (CC BY-NC-ND 4.0, <https://creativecommons.org/licenses/by-nc-nd/4.0/>), which permits use, distribution, and reproduction in any medium, provided that the Article is properly cited, the use is non-commercial, and no modifications or adaptations are made.



# CAUCHY-BASED MODELLING IN CEMENTITIOUS MATERIALS TECHNOLOGY

P. STROEVEN<sup>1</sup>, M. SŁOWIK<sup>2</sup>

Cauchy paved the way for constructing models in concrete technology, and elsewhere. He determined the (non-flat) surface area in 3D by measuring random total projections. Analogously, he determined the length of a curved line in 2D by way of measuring the total projections. The paper will present the mathematical expressions, because in many branches of concrete technology, modelling is found based on such Cauchy concepts. These branches – fractography in compression, tension or shear, fibre reinforcement and permeability estimation – will briefly be mentioned to demonstrate this. It has been found that, for the discussed fields of engineering relevance, major model parameters for cementitious materials are similar to those developed by Cauchy in the 19<sup>th</sup> century. In the paper some previous investigations concerning fractography, fibre reinforcement and fracture roughness will be summarized but basically a new development on porosimetry will be presented. Particularly a new achievement of successful implementation of the methodology (also based on Cauchy) for optimizing permeability estimation will be discussed.

*Keywords:* Cauchy concepts, fractography, fibre reinforcement, fracture roughness, pore tortuosity, permeability

<sup>1</sup> Prof., PhD., Eng., Delft University of Technology, Faculty of Civil Engineering and Geosciences, Stevinweg 1, 2628 CN Delft, the Netherlands, e-mail: p.stroeven@tudelft.nl

<sup>2</sup> DSc., PhD., Eng., Lublin University of Technology, Faculty of Civil Engineering and Architecture, Nadbystrzycka 40, 20-618 Lublin, Poland, e-mail: m.slowik@pollub.pl

## 1. INTRODUCTION

Cauchy paved the way for constructing models in concrete technology, and elsewhere. He determined the (non-flat) surface area in 3D by measuring random total projections (hence in 2D). Analogously, he determined the length of a curved line in 2D by way of measuring the total projections (hence in 1D). The paper will present the mathematical expressions, because in many branches of concrete technology, modelling is found based on such Cauchy concepts. In the paper it has been demonstrated that several modelling activities connected with concrete technology are governed by two constants of Cauchy, *i.e.*,  $1/2$  and  $2/\pi$ . In particular this holds for branches as fractography in compression (or tension), fibre reinforcement, fracture roughness in shear and pore tortuosity for permeability estimation, which are briefly introduced.

An extensive literature is available on the fractography and fibre reinforcement topics, so only a limited number of publications is referred to that discuss many of the international contributions to the field. An exception is the field of porosimetry for permeability estimation that is still being developed. Herein we also present limited contributions to the field. The hard-core of this publication is revealing their joint Cauchy basis.

In the paper some previous investigations will be summarized but basically a new development on porosimetry will be presented. Particularly a new achievement of successful implementation of the methodology (also based on Cauchy) for optimizing permeability estimation will be presented. It was also recently discussed by the authors in [23].

## 2. CAUCHY FORMULAS

The mathematical expressions derived by Cauchy relates the surface area in space,  $S$ , to the average planar total projected area,  $A'$ , and, analogously, the length of the line in a plane,  $L$ , to the average projected linear line length,  $L'$ . For spatial averaging, two independent angles are necessary, say  $\beta$  and  $\theta$ . The averaging is conducted over  $\{\beta, \sin\theta\}$ . Further,  $\cos\theta$  is involved to account for the projection action. Hence, surface area in space,  $S$ , is related to the average planar total projected area,  $A'$ , by Eq. 2.1 and, analogously, for the 2D case by Eq. 2.2, both due to Cauchy [2]:

$$(2.1) \quad \bar{A}' = S \frac{\int_0^{\pi/2} \sin \theta \cos \theta d\theta}{\int_0^{\pi/2} \sin \theta d\theta} = \frac{1}{2} S$$

$$(2.2) \quad \bar{L}' = L \frac{\int_0^{\pi/2} \cos \beta d\beta}{\int_0^{\pi/2} d\beta} = \frac{2}{\pi} L$$

where the angle over which is projected is  $\beta$ .  $L$  is the length of the line in the plane and  $L'$  is the average projected linear line length. The situation is sketched in Fig. 1 [21]. We will see that many of the modelling activities will be governed by these two constants of Cauchy, *i.e.*,  $1/2$  and  $2/\pi$ !

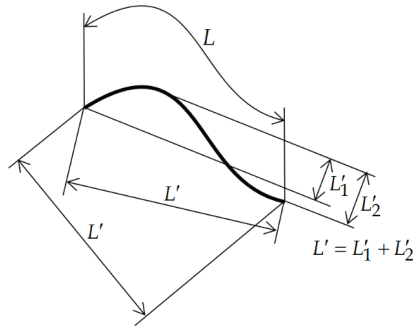


Fig. 1. Total projection of a curved line (dark black) in a plane in different directions,  $L'$ , respectively.

Total projection means in some cases a double projection as indicated at the right.

### 3. FRACTOGRAPHY

In fractography, we strive for the assessment of quantitative measures for damage or cracking. Yet, this is a phenomenon hidden by the opaque nature of the concrete. As a consequence, we have to rely on sections cut through the material. Fig. 2 at the left reveals an enlarged part of such a section in which the cracks are visualized by a fluorescent spray and thereupon photographing under UV light. The hand copied full section pattern of cracks, visualized in this way, is shown at the right.

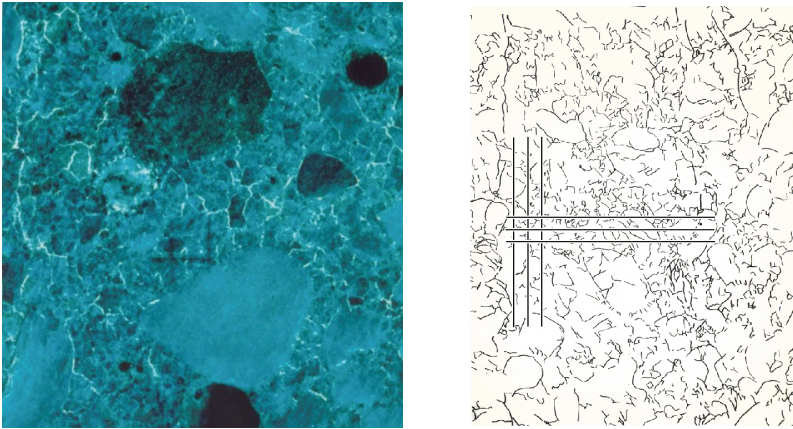


Fig. 2. (left) Part of the section image of a pre-loaded prismatic concrete specimen in compression reveals myriads of small cracks that are visualized by the fluorescent spray technique before hand-copying; (right) Manually copied crack pattern of a complete, centrally located axial section.

The loading case is direct compression, so the common assumption is that the special crack system will be partly governed by an isotropic uniform random (IUR) portion of cracks (shortly: 3D portion) and another portion that is parallel to the loading axis (shortly: 1D portion). As a consequence, the crack pattern at the right reveals a mixture of cracks cut by the section plane and originating from the 3D and the 1D portions. The cutting of the first is found governed by the Cauchy constant  $1/2$ , whereas the second portion by the Cauchy constant  $2/\pi$ ! In mathematical terms, it is found that the crack surface area per unit of volume,  $S_V$ , is related to orthogonal measurements in the mid-section of the compressed specimen by:

$$(3.1) \quad S_V = \frac{\pi}{2} \left( P_L(hor) + \left( \frac{4}{\pi} - 1 \right) P_L(vert) \right)$$

whereby we applied the “Stroeven” concept that says that the real crack structure is a *linear* combination of a 3D and 1D components. Hence, only a single section in the direction of that of the compressive load is required and a set of two orthogonal measurements by grids of parallel lines, with  $P$  as the number of intersection with cracks and  $L$  as the total line length (see Fig. 2). When solely confronted with 3D cracking, whereby the horizontal and vertical measurements are equal, the result is  $S_V = P_L/2$ . Note the Cauchy constant of  $1/2$ ! Similarly, for only 1D cracking, we have  $S_V = \pi P_L(hor)/2$  and the second Cauchy constant of  $2/\pi$  is obtained! Hence, modelling for assessing cracking in

concrete specimens relies on Cauchy, the demonstration of which was the target of this paper. With a mixture of 2D and 3D cracks for modelling cracking in *direct tension*, we can proceed similarly, confirming the above statement [13,14,15].

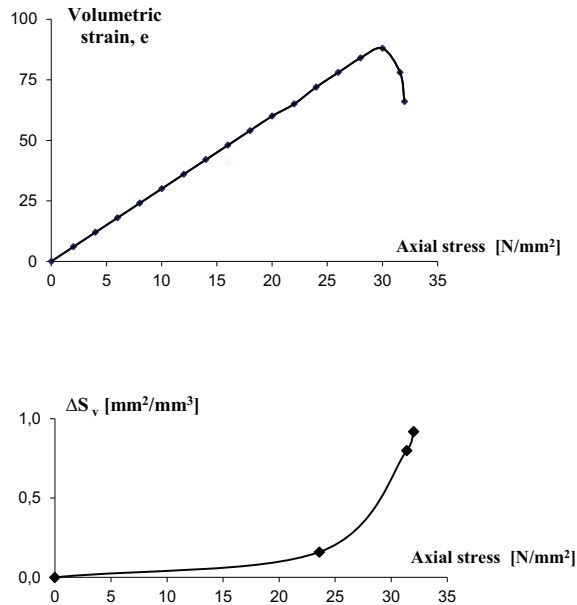


Fig. 3. Development in prismatic specimens under direct compression of crack surface area per unit of volume,  $S_V$ , and volumetric strain,  $e = (\varepsilon_x + \varepsilon_y + \varepsilon_z) / 3$ , both as a function of axial stress,  $\sigma_x$ .

Applications can be found in [7,9,13]. Fig. 3 shows a direct application of Eq. 3.1 in compression testing research. The top of Fig. 3 presents the development of volumetric strain,  $e$ , vs axial stress. At the bottom, the increase in crack surface area per unit volume during the development of  $e$  is depicted. The discontinuity in the  $\Delta S_V$  curve is significantly before the top in the  $e$ -curve. The first can be associated with breaking down by local shear of the “en échelon” crack arrays at the top of the (specifically, larger) aggregate grains. For details, see [5, 9,15,21].

#### 4. FIBRE REINFORCEMENT

Steel fibres are employed for reinforcement in concrete. Of course, they only transfer stress when favourably oriented with respect to the stress field. This has been investigated on specimens tested for mechanical behaviour. This was achieved both by counting fibres in sections or, alternatively, by making X-ray photographs of tiles cut from the specimen. An example of the latter is displayed in Fig. 4. Assuming a mixture of 2D and 3D fibre portions (according to the “Stroeven” concept), the following equation is obtained [10,20]:

$$(4.1) \quad L_V' = \left[ \left( \frac{1}{2} + \left( \frac{2}{\pi} - \frac{1}{2} \right) \omega \right) \right] L_V$$

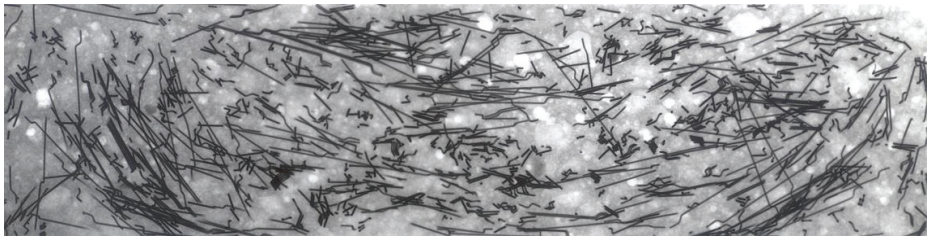


Fig. 4. X-ray radiograph of “vertical slice” of SFRC specimen of 70x200x1000 mm; gravitation during compaction was in vertical direction (perpendicular to top surface) [11,12,16].

Herein,  $\omega$  is the total length ratio of the 2D fibre oriented portion over that of the total amount of fibres. Mono-size fibres are assumed in this case, however, also for multi-size and curved fibres, similar models have been expanded. In eq. (4.1),  $L_V$  is the total fibre length per unit of volume and  $L_V'$  the component in the plane of the 2D component, so, in the case of Fig. 4, in the loading direction of the prismatic specimen perpendicular to the image. Consequently, it is the effective part of the fibre reinforcement. We see that for  $\omega=0$  (only 3D fibre dispersion), respectively, for  $\omega=1$  (only 2D fibre dispersion), we obtain – again - the Cauchy constants  $1/2$  and  $2/\pi$ . Note, finally, that for counting fibres in sections, formulas are available also based on Cauchy constants [10].

As promised earlier, here is the derivation of the Cauchy constant in the 3D case of fibre dispersion. Fibres of different length are subdivided in *unit line elements*. This strategy is also followed for curved fibres. The assumption is that these unit length fibre elements are isotropic uniformly random (IUR) dispersed; this is what we normally denote as “random”. The end points of the unit sub-length of

these fibres cover UR the surface area of the unit sphere in Fig. 5. The average projected length of  $L$  along an axis of the sphere, in the present case the z-axis, is given by:

$$(4.2) \quad \bar{L}' = L \frac{\int_0^{\pi/2} \int_0^{\pi/2} \sin \theta \cos \theta d\theta d\beta}{\int_0^{\pi/2} \int_0^{\pi/2} \sin \theta d\theta d\beta} = \frac{1}{2} L$$

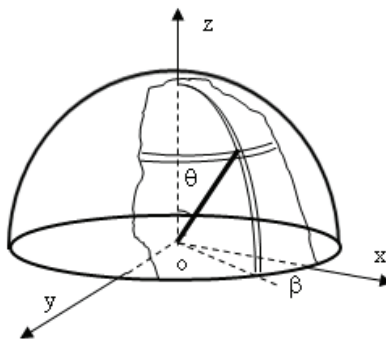


Fig. 5. Visualization by unit sphere model of orientation distribution of mono-size fibre elements in SFRC specimen. Fibre elements are considered translated from bulk to join in one of their ends in point O.

As a consequence, other ends will UR cover the surface of the sphere with unit radius,  $L$ .

## 5. ROUGHNESS OF FRACTURE SURFACES IN SHEAR

The planar roughness index,  $R_s$ , is defined as the total surface area of the structure obtained by pull out of all aggregate grains in the concrete intersecting a dividing plane,  $S$ , shown in Fig. 6 at the left, divided by the area of the dividing plane,  $A$ . Hence  $R_s = S/A$ . For convenience of modelling, all particles are assumed spherical. The following expression is readily obtained for a non-flat fracture surface [17,18]:

$$(5.1) \quad R_s = 1 - V_V + 3V_{V3} + \frac{3}{2}V_{V2} = 1 + 2V_V \left(1 - \frac{3}{4}\omega\right)$$

Herein,  $V_V$  is the volume fraction of aggregate. For  $\omega=1$ , the 3D component is absent and a flat dividing plane is obtained of which the planar surface roughness index is given by  $R_s = V_V/2$ .

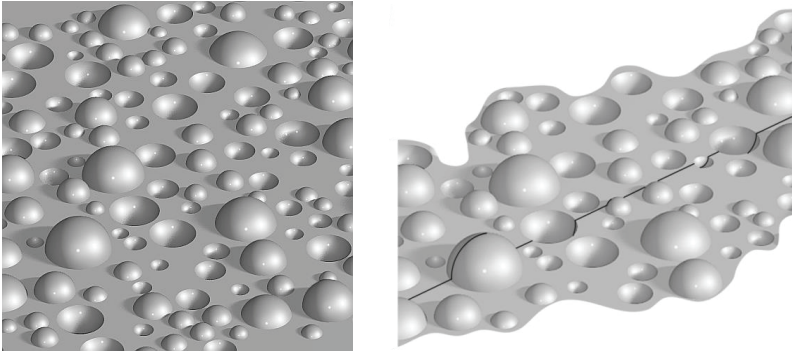


Fig. 6. Meso-scale model of dividing plane through concrete and supposedly spherical aggregate particles under load released from matrix due to interface cracking.

The linear roughness index,  $R_l$ , is the length of a vertically projected line on the structure at the left. The result is depicted at the right. The associated approximate expression for the linear roughness index is (for  $\omega=1$ )

$$(5.2) \quad R_l \approx 1 + \frac{\pi}{2} V_V \left( \frac{1}{4} \right)$$

The Cauchy constants in these expressions are apparent!

The planar roughness index could be a useful parameter in shear studies. The expressions are used, of course in fractography. The linear roughness index is additionally employed in porosimetry for the assessment of the pore tortuosity effect on permeability.

## 6. PORE TORTUOSITY FOR PERMEABILITY ESTIMATION

Pore tortuosity can readily be obtained on a virtual representation of the material (compconcrete) by DRaMuTS. In [17,18], the linear tortuosity index  $R_l$  (Eq. 5.2) is developed on meso-level for a “random” structure of spherical aggregate particles (Fig. 6) in which the volume fraction of particles  $V_V$  could be replaced on the micro-level by  $(1-p)$ , with  $p$  as porosity. This is to account for interferences of hydrating spherical cement particles. Hence, we have as reference formula:

$$(6.1) \quad R_l \approx 1 + \frac{\pi}{2}(1-p) = \frac{l}{l'}$$

whereby  $l$  and  $l'$  represent the real length of the pore channel and the straight line connecting the places where the pore channel intersects the external opposite surfaces of the cement paste element in the virtual representation of the cementitious material. Fig. 6 depicts the underlying model [17, 18]. Note that in defining the tortuosity index, also the squared value of  $l/l'$  is in use as well as the planar tortuosity index. In the present, meso-level approach, the projected line is partly in the dividing plane and for the rest *projected vertically* from the surfaces of the grains to this plane (for the present purpose, the hydrate clusters) intersecting with the dividing plane. First of all, the connecting line element between the nodes will in reality constitute a 3D dispersion and not a 2D one that is underlying Eq. (6.1). Further, roughly speaking, the tortuous line and the straight line connecting the points at beginning and end of this tortuous line are never far away from each other. This is certainly not a very realistic concept as demonstrated by Fig. 7, at the right. Predictions of Eq. (6.1) for  $p=0.4$  (high  $w/c$ ; early hydration stage) amount to  $R_l \sim 2$  and for  $p=0.1$  (advanced pore depercolation)  $R_l=2.4$ . Hence, tortuosity increases with pore depercolation, however not in a very dramatic way.

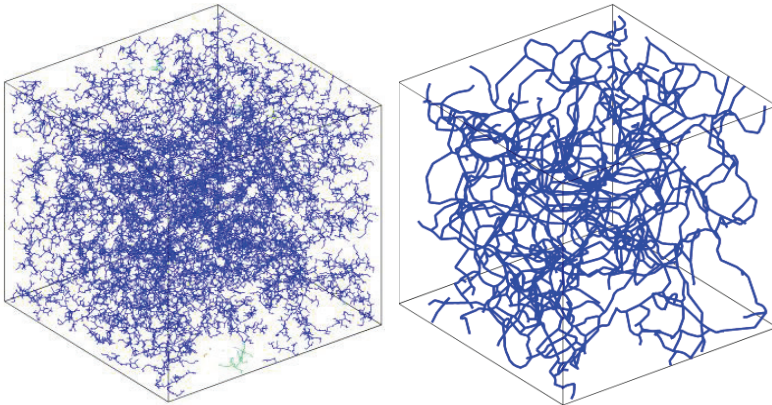


Fig. 7. (left) All pores in 90 days hydrated cement paste with  $w/c = 0.4$  and Blaine surface area of  $300 \text{ m}^2/\text{kg}$ . Porosity is 19%. (right) Continuous pores only – obtained by DRaMuTS.

The formulas developed in fractography (Eq. 3.1) and fiber reinforcement (Eq. 4.1) can be used directly to predict tortuosity of the capillary pores in the network structure. They lead to the estimation of tortuosity between  $\pi/2$  and 2. This is precisely what has been found in experiments [1, 3,6,8,24]. Our research shows that for water saturation degrees met in engineering practice of concrete

structures, pore tortuosity will be closer to 2. This can be imagined from the pore network structure shown in Fig. 7.

For completeness sake, it should be mentioned that the standard porosimetry approach to virtual cementitious materials provides numerical data obtained by way of the tube network that is a simpler schematization of the pore network shown in Fig. 7. The porosimetry approach encompasses “measuring” pore size in  $2 \times 10^6$  “randomly” dispersed points (of which only those inside pores are employed). The measuring is conducted by stars in all points inside pores. The smallest pore section in each dispersed point (throat) is obtained by 2D star probing in about 200 sections. In each point, large numbers of star pikes are measured. Since this is not the hard core of this paper, the interested reader is referred to details of the methodology available in [4]. This so called throat size is fed into the tube network, together with the pore length between the points. The complete calculus lasts about 1 hour.

Relevant for this paper are two developments aiming to optimize estimating permeability. In the first, instead of determining all sizes of the pore throats, we disperse isotropic uniform random (IUR) sections over the relevant pores. Hence the size of only one given section per point is determined by 2D star probing. It is found that the median pore size obtained from the throat size distribution function is directly related to the median pore size obtained from the “random” section pore size distribution function. For the proof, Cauchy’s concept of random projection of a surface area is employed (Eq. 2.1). For the proof see [22]. As a result, the median pore areas differ by the Cauchy constant of 2 (and thus the pore radii of the representative pore circles by  $\sqrt{2}$ ). This reduces the required efforts by 85%.

The second development in a globalized approach to permeability estimation is combining this contracted approach to pore size assessment with the tortuosity concept, discussed above. A paper on this topic is in preparation.

## 7. CONCLUSIONS

At designing models for cementitious materials, it is indeed found that for the discussed fields of engineering relevance major model parameters are similar to those developed quite a long time ago by Cauchy forming a sound methodological basis for such modelling approaches. That was the very target of this paper. Moreover, the Cauchy concepts offer possibilities for further structural modelling, such as the economic porosimetry approaches in virtual reality indicated herein.

## REFERENCES

1. Bathia, S.K. Directional autocorrelation and diffusional tortuosity of capillary porous media. *J. Catalysis*, 93: 192-196, 1985.
2. Cauchy, A. "Mémoires sur rectification des courbes et la quadrature des surfaces courbes", Cambridge University Press, Cambridge, UK. (in French), 1882.
3. Haughey, D.P., Beveridge, G.S.G. Structural properties of patched beds. *Can. J. Chem. Eng.*, 47:130-140, 1969.
4. Le, L.B.N. "Micro-level porosimetry of virtual cementitious materials. Structural impact on mechanical and durability evolution", PhD Thesis, Delft University of Technology, the Netherlands, 2015.
5. Perry, C., Gillott, J.E. The influence of mortar aggregate bond strength on the behaviour in compression. *Cem. Concr. Res.*, 7: 553-564, 1977.
6. Peterson, E.E. Diffusion in a pore of varying cross section. *Am. Inst. Chem. Eng.*, 4: 343-345, 1958.
7. Reinhardt, H.W., Stroeven, P., Uijl J.A. den, Kooistra, T.R., Vrencken, H.A.M. Einfluss van Schwingbreite, Belastungshöhe und Frequenz auf die Schwingfestigkeit von Beton bei niedrigen Bruchlastwechselzahlen *Betonw. + Fertigt. Techn.*, 9: 498-503, 1978.
8. Sobieski, W. The use of path tracking method for determining the tortuosity field in a porous bed. *Gran. Mats.*, 18: 72, 2016.
9. Stroeven, P. "Some aspects of the micromechanics of concrete", PhD Thesis, Delft University of Technology, the Netherlands, 1973.
10. Stroeven, P. Morphometry of fibre reinforced cementitious materials. Part II: Inhomogeneity and anisometry of partially oriented fibre structures. *Mat. Struct.*, 12(67):9-20, 1978.
11. Stroeven, P., Shah, S.P. Use of radiography-image analysis for steel fibre reinforced concrete. In : Testing and test methods of fibre reinforced composites. Constr. Press, Lancaster: 345-353, 1978.
12. Stroeven, P. Micro- and macro-mechanical behaviour of steel fibre reinforced mortar in tension. *Heron*, 24(4): 7-40, 1979a.
13. Stroeven, P. Geometric probability approach to the examination of microcracking in plain concrete. *J. Mat. Sci.*, 14: 1141-1151, 1979b.
14. Stroeven, P. Some observations on microcracking in concrete subjected to various loading regimes. *Eng. Fract. Mech.*, 35(4/5): 775-782, 1990.
15. Stroeven, P. Damage mechanisms in fibre reinforced concrete composites. In: *Comptes rendus des neuvièmes journées nationales sur les composites* (AMAC, France, Saint-Étienne): 925-938, (in French), 1994.
16. Stroeven, P., Dalhuisen, D.H. Damage evolution characteristics of steel fibre reinforced concrete in direct tension. *Engrn. Mech.*, 3(4): 273-280, 1996.
17. Stroeven, P. Stereological estimates for roughness and tortuosity in cementitious composites. *Im. Anal. Stereol.*, 19: 67-70, 2000.
18. Stroeven, P. A stereological approach to roughness of fracture surfaces and tortuosity of transport paths in concrete. *Cem. Concr. Comp.* 22: 331-341, 2000.
19. Stroeven, P., Hu, J. Review paper – stereology : Historical perspective and applicability to concrete technology. *Mat. Struct.*, 39:127-135, 2006.
20. Stroeven, P. Stereological principles of spatial modeling applied to steel fibre-reinforced concrete in tension. *ACI Mat. Journ.*, 106(3): 1-10, 2009.
21. Stroeven, P. 50 Years' focus on concrete: from meter- to nano-scale 1963-2013. Media Center, Rotterdam, 2015.
22. Stroeven, P., Li, K. A modern approach to porosimetry of virtual cementitious materials. *Mag. Concr. Res.*, 69(23): 1212-1217, 2017.
23. Stroeven, P., Slowik, M. Economic and reliable estimation of cementitious materials properties on the basis of virtual models. In: *Brittle Matrix Composites 12* (Eds Glinicki M.A., Józwiak-Niedźwiecka D., Leung C.K.Y., Olek J.), Institute of Fundamental Technological Research: 35-44, 2019.
24. Sun, G.W., Sun, W., Zhang, Y.S., Liu, Z.Y. Relationship between chloride diffusivity and pore structure of hardened cement paste. *J. Zhejiang Univ. Sci. A*, 12(5): 360-367, 2011.

## LIST OF FIGURES

Fig. 1. Total projection of a curved line (dark black) in a plane in different directions,  $L'$ , respectively. Total projection means in some cases a double projection as indicated at the right.

Fig. 2. (left) Part of the section image of a pre-loaded prismatic concrete specimen in compression reveals myriads of small cracks that are visualized by the fluorescent spray technique before hand-copying; (right) Manually copied crack pattern of a complete, centrally located axial section.

Fig. 3. Development in prismatic specimens under direct compression of crack surface area per unit of volume,  $S_V$ , and volumetric strain,  $e = (\varepsilon_x + \varepsilon_y + \varepsilon_z) / 3$ , both as a function of axial stress,  $\sigma_x$ .

Fig. 4. X-ray radiograph of “vertical slice” of SFRC specimen of 70x200x1000 mm; gravitation during compaction was in vertical direction (perpendicular to top surface) [11,12,16].

Fig. 5. Visualization by unit sphere model of orientation distribution of mono-size fibre elements in SFRC specimen. Fibre elements are considered translated from bulk to join in one of their ends in point O. As a consequence, other ends will UR cover the surface of the sphere with unit radius,  $L$ .

Fig. 6. Meso-scale model of dividing plane through concrete and supposedly spherical aggregate particles under load released from matrix due to interface cracking.

Fig. 7. (left) All pores in 90 days hydrated cement paste with  $w/c = 0.4$  and Blaine surface area of 300 m<sup>2</sup>/kg. Porosity is 19%. (right) Continuous pores only – obtained by DRaMuTS.

Received 04.09.2019, Revised 21.04.2020